


Electron-impact single, double, and triple ionization of B⁺Jurgita Koncevičiūtė* and Valdas Jonauskas *Institute of Theoretical Physics and Astronomy, Vilnius University, Saulėtekio av. 3, LT-10257 Vilnius, Lithuania*

(Received 17 May 2020; accepted 12 July 2021; published 11 October 2021)

Electron-impact single, double, and triple ionizations are investigated for the B⁺ ion. The direct and indirect ionization processes are studied for the single and double ionization. Good agreement with measurements for the single and double ionization is obtained when the scaled distorted-wave cross sections are used to study the collisional ionization and excitation processes. It is shown that ionization-excitation-autoionization and excitation-ionization-autoionization processes have to be introduced to the total double ionization to explain the measurements. The triple ionization is investigated by considering the direct double ionization with the subsequent autoionization.

DOI: [10.1103/PhysRevA.104.042804](https://doi.org/10.1103/PhysRevA.104.042804)**I. INTRODUCTION**

Electron-impact single and multiple ionization processes have been the focus of many theoretical and experimental studies. These processes provide fundamental understanding of the electronic dynamics and structure of atoms and ions. Information about such small systems can be obtained by perturbing the system under investigation. Collisions of the atomic systems with electrons is a typical method for such studies. Products of these processes are singly and multiply ionized ions, which can be measured directly in experiments. Multiple ionization has considerable impact on charge-state distribution in the environments with high abundances of energetic electrons [1,2]. The study of the multiple ionization processes is quite complicated as one has to deal, at least, with the four-body Coulomb problem.

Being one of the three light elements (Li, Be, and B) that are not effectively synthesized by nuclear reactions in stable stars, boron is scarce in the solar system and in stars, and its abundances are low compared to neighboring elements on the periodic table [3]. However, this element is important in fusion devices where the plasma-induced deposition of boron-containing films on the plasma-exposed surfaces (boronization) is used as a powerful wall conditioning method to achieve very pure fusion plasmas [4,5]. In order to understand erosion processes of the neutral and ionized boron in fusion experiments, such as the International Thermonuclear Experimental Reactor, comprehensive data for electron collisions with these ions are needed. These data will include not only the collisions with atoms and ions in their ground state, but also involving excited states.

Nonperturbative calculations have been previously completed for electron-impact ionization of the B atom [6,7] as well as the B⁺ [8] and B²⁺ [9] ions in their ground and metastable states. The single ionization (SI) cross sections were obtained using crossed-beams experiments for the B⁺ ion [8,10]. Electron-impact double ionization (DI) of the

B⁺ ion has been previously studied by applying nonperturbative time-dependent close-coupling (TDCC) method for the direct double ionization (DDI) process and perturbative time-independent distorted-wave (DW) approximation for the indirect DI processes [11]. However, the TDCC calculations are available only in the range of incident energies between the DDI threshold and the inner-shell SI threshold. Theoretical studies are presented here for the triple ionization (TI) process of the B⁺ ion.

The aim of this paper is to investigate electron-impact SI, DI, and TI processes for the B⁺ ion. The role of direct and indirect processes for SI and DI is analyzed. The DDI process is studied using a multi-step approach [12–15] which involves ionization-ionization (II), excitation-ionization-ionization (EII), and ionization-excitation-ionization (IEI) processes. In addition to these processes, other two-step processes are considered in the study of DI. The additional processes include ionization-excitation-autoionization (IE-AI) and excitation-ionization-autoionization (EI-AI). The TI is studied as DDI with the subsequent autoionization (DDI-AI). The correlation effects are included for the ground configuration of the B⁺ ion using the configuration interaction method.

The rest of the paper is structured as follows. In Sec. II, an overview of the theoretical approach is given; single, double, and triple electron-impact ionization cross sections for the B⁺ ion are presented and compared with available experimental measurements in Sec. III; a brief summary with some final conclusions are provided in Sec. IV.

II. THEORETICAL APPROACH

Different mechanisms are responsible for the formation of single, double, and triple ionization processes. The contribution of these mechanisms differs at various energies of the impacting electron. Further in this section, the miscellaneous mechanisms involved in the single, double, and triple ionization processes of the B⁺ ion are presented.

Direct and indirect electron-impact ionization processes contribute to the total electron-impact SI. The total electron-

*Jurgita.Konceviciute@tfai.vu.lt

impact SI cross section σ^{SI} from the level i of the initial ion to the level f of the singly ionized ion can be expressed as a sum of the direct and indirect ionization cross sections by the equation,

$$\sigma_{if}^{\text{SI}}(\varepsilon) = \sigma_{if}^{\text{CI}}(\varepsilon) + \sum_j \sigma_{ij}^{\text{CE}}(\varepsilon) B_{jf}^a, \quad (1)$$

here $\sigma_{if}^{\text{CI}}(\varepsilon)$ is the cross section for the single collisional ionization (CI), ε is an energy of the incident electron, term $\sum_j \sigma_{ij}^{\text{CE}}(\varepsilon) B_{jf}^a$ corresponds to the indirect ionization cross section, where $\sigma_{ij}^{\text{CE}}(\varepsilon)$ is the collisional excitation (CE) cross section to the intermediate level j of the initial ion, B_{jf}^a is a branching ratio for the autoionization process from the level j to the final level f . The branching ratio represents a radiative damping of the indirect process and can be expressed by the equation,

$$B_{jf}^a = \frac{A_{jf}^a}{\sum_m A_{jm}^a + \sum_n A_{jn}^r}, \quad (2)$$

where A^a and A^r are the Auger and radiative transition probabilities, respectively.

DI can occur via direct and indirect processes as in case of SI. The total DI cross sections can be obtained by summing up the direct and indirect terms,

$$\sigma_{if}^{\text{DI}}(\varepsilon) = \sigma_{if}^{\text{DDI}}(\varepsilon) + \sum_j \sigma_{ij}^{\text{CI}}(\varepsilon) B_{jf}^a, \quad (3)$$

where σ_{if}^{DDI} is the DDI cross section and a term $\sum_j \sigma_{ij}^{\text{CI}}(\varepsilon) B_{jf}^a$ describes the indirect double ionization process: ionization with subsequent autoionization (IA) through the intermediate level j of the ionized ion.

The previously proposed multistep approach [12–15] is used to study electron-impact DDI cross sections for the B^+ ion. This approach deals with DDI as a sum of the II, IEI, and EII paths. The same approach was also applied to study double and triple Auger transitions in C^+ [16]. Two limiting cases of the energy distribution for the scattered and ejected electrons were analyzed in the previous studies [12–15]. In previous DI studies, it has been demonstrated that a better agreement with measurements at higher energies of the incident electron in the DDI process for the light ions Li^+ [13], O^+ , O^{2+} , O^{3+} , C^{1+} , and Ar^{2+} [12] was obtained when it was assumed that after the initial single ionization process the scattered and ejected electrons share the excess energy equally. However, it has also been shown that mainly one of the electrons takes all the excess energy and participates in the further processes at the lower energies of the incident electron. In the current paper, the distribution of the excess energy between the scattered and the ejected electrons from the first ionization process is estimated by using the differential cross sections obtained from the binary-encounter-dipole (BED) model [17]. This approach was implemented to study multiple Auger transitions [18–20] and ionization by electron impact [21]. The equation for the DDI process from level i to level f through the II path, which involves two sequential CI processes, can be written as

$$\sigma_{if}^{\text{DDI(II)}}(\varepsilon) = \sum_j \sigma_{ij}^{\text{CI}}(\varepsilon) \int_{E_{ij}}^{\varepsilon - E_{ij}} \rho_{ij}(\varepsilon, \varepsilon_1) \frac{\sigma_{jf}^{\text{CI}}(\varepsilon_1)}{4\pi \bar{R}_{nl}^2} d\varepsilon_1, \quad (4)$$

here E_{ij} is a transition energy, and ε_1 is an energy of the scattered or ejected electron. One of these electrons in the further step collides with one of the remaining bound electrons from the nl subshell and ejects it. The energy distribution $\rho_{ij}(\varepsilon, \varepsilon_1)$ is normalized to unity: $\int_0^{\varepsilon - E_{ij}} \rho_{ij}(\varepsilon, \varepsilon_1) d\varepsilon_1 = 1$. A probability of the second electron-impact ionization process is represented by a factor $\int_{E_{ij}}^{\varepsilon - E_{ij}} \rho_{ij}(\varepsilon, \varepsilon_1) \frac{\sigma_{jf}^{\text{CI}}(\varepsilon_1)}{4\pi \bar{R}_{nl}^2} d\varepsilon_1$; the factor $\frac{\sigma_{jf}^{\text{CI}}(\varepsilon_1)}{4\pi \bar{R}_{nl}^2}$ represents the probability of the ionization process by the electron with energy ε_1 . The term \bar{R}_{nl} describes the mean distance of the electrons from the nucleus.

The EII process, which involves electron-impact excitation followed by two sequential CIs, is another possible path leading to DDI. Cross sections of this process can be expressed by the equation,

$$\begin{aligned} \sigma_{if}^{\text{DDI(EII)}}(\varepsilon) &= \sum_{jk} \sigma_{ij}^{\text{CE}}(\varepsilon) \frac{\sigma_{jk}^{\text{CI}}(\varepsilon - E_{ij})}{4\pi \bar{R}_{nl}^2} \\ &\times \int_{E_{kf}}^{\varepsilon - E_{ij} - E_{jk}} \rho_{jk}(\varepsilon - E_{ij}, \varepsilon_1) \frac{\sigma_{kf}^{\text{CI}}(\varepsilon_1)}{4\pi \bar{R}_{n'l'}^2} d\varepsilon_1. \end{aligned} \quad (5)$$

Another three-step process, through which DDI can occur, is the IEI path. This path involves CI followed by an excitation with subsequent ionization. Cross sections of this process are written as

$$\begin{aligned} \sigma_{if}^{\text{DDI(IEI)}}(\varepsilon) &= \sum_{jk} \sigma_{ij}^{\text{CI}}(\varepsilon) \int_{E_{jk}}^{\varepsilon - E_{ij}} \rho_{ij}(\varepsilon, \varepsilon_1) \\ &\times \frac{\sigma_{jk}^{\text{CE}}(\varepsilon_1) \sigma_{kf}^{\text{CI}}(\varepsilon_1 - E_{jk})}{4\pi \bar{R}_{nl}^2 4\pi \bar{R}_{n'l'}^2} d\varepsilon_1, \end{aligned} \quad (6)$$

here $\frac{\sigma_{kj}^{\text{CE}}(\varepsilon_1)}{4\pi \bar{R}_{nl}^2}$ is the excitation probability of electron from the nl subshell of level k to level j by the scattered or ejected electron with energy ε_1 .

In addition to previously described IA process, other indirect processes are introduced for DI of the B^+ ion in this paper. These processes include ionization-excitation followed by an autoionization (IE-AI) and excitation-ionization with subsequent autoionization (EI-AI). An equation of the DI process through the IE-AI path can be written as

$$\sigma_{if}^{\text{DI(IE-AI)}}(\varepsilon) = \sum_{jk} \sigma_{ij}^{\text{CI}}(\varepsilon) \int_{E_{jk}}^{\varepsilon - E_{ij}} \rho_{ij}(\varepsilon, \varepsilon_1) \frac{\sigma_{jk}^{\text{CE}}(\varepsilon_1)}{4\pi \bar{R}_{nl}^2} d\varepsilon_1 B_{kf}^a. \quad (7)$$

Similarly, the equation of the DI process through the EI-AI path can be written as

$$\sigma_{if}^{\text{DI(EI-AI)}}(\varepsilon) = \sum_{jk} \sigma_{ij}^{\text{CE}}(\varepsilon) \frac{\sigma_{jk}^{\text{CI}}(\varepsilon - E_{ij})}{4\pi \bar{R}_{nl}^2} d\varepsilon_1 B_{kf}^a. \quad (8)$$

If the energy of the excited level produced by the DDI process is higher than the TI threshold, this level can decay further via autoionization (DDI-AI) to the next ionization stage. The autoionization after DDI leads to TI. Therefore, the electron-impact TI process in this paper is studied as a sum of the DDI(II)-AI, DDI(IEI)-AI, and DDI(EII)-AI processes.

Equations for the DDI process formed by the II, EII, and IEI paths with subsequent autoionization from level i of the initial ion to level f of the triply ionized ion can be written as

$$\sigma_{if}^{\text{DDI(II)-AI}}(\varepsilon) = \sum_j \sigma_{ij}^{\text{DDI(II)}}(\varepsilon) B_{jf}^a, \quad (9)$$

$$\sigma_{if}^{\text{DDI(EII)-AI}}(\varepsilon) = \sum_j \sigma_{ij}^{\text{DDI(EII)}}(\varepsilon) B_{jf}^a, \quad (10)$$

$$\sigma_{if}^{\text{DDI(IEI)-AI}}(\varepsilon) = \sum_j \sigma_{ij}^{\text{DDI(IEI)}}(\varepsilon) B_{jf}^a, \quad (11)$$

where DDI is described by two- and three-step processes from level i of the initial ion to level j of the B^{3+} ion [Eqs. (4)–(6)].

The autoionization process following DDI is represented in Eqs. (9)–(11) by the branching ratio B_{jf}^a from level j of the B^{3+} ion to level f of B^{4+} .

The indirect process of DI includes ionization from the $1s$ subshell with subsequent autoionization,

$$1s^2 2s^2 + e^- \rightarrow 1s 2s^2 + 2e^- \rightarrow 1s^2 + 3e^-. \quad (12)$$

For the $2s$ subshell, the DDI II process is defined by the sequential CI,

$$1s^2 2s^2 + e^- \rightarrow 1s^2 2s + 2e^- \Rightarrow 1s^2 + 3e^-. \quad (13)$$

The ionization or excitation by the scattered or ejected electrons is shown by the \Rightarrow symbol. The DDI EII process presents CE with sequential CI of the valence subshells,

$$1s^2 2s^2 + e^- \rightarrow 1s^2 2s nl + e^- \Rightarrow \begin{cases} 1s^2 2s \\ 1s^2 nl \end{cases} + 2e^- \Rightarrow 1s^2 + 3e^-, \quad (14)$$

where $n \leq 10$, $l < n$, and $l \leq 5$. The DDI IEI process can be schematically shown as

$$1s^2 2s^2 + e^- \rightarrow 1s^2 2s + 2e^- \Rightarrow 1s^2 nl + 2e^- \Rightarrow 1s^2 + 3e^-. \quad (15)$$

The DDI process that involves the $1s$ subshell is studied separately since this subshell was not investigated before [11]. DDI II which includes the $1s$ subshell of B^{2+} is defined as

$$1s^2 2s^2 + e^- \rightarrow 1s^2 2s + 2e^- \Rightarrow 1s 2s + 3e^-. \quad (16)$$

In this case, DDI EII starts by the excitation from the $2s$ subshell,

$$1s^2 2s^2 + e^- \rightarrow 1s^2 2s nl + e^- \Rightarrow \begin{cases} 1s^2 2s \\ 1s^2 nl \end{cases} + 2e^- \Rightarrow \begin{cases} 1s 2s \\ 1s nl \end{cases} + 3e^-, \quad (17)$$

The DDI IEI process includes the excitation from the $1s$ subshell of the B^{2+} ion,

$$1s^2 2s^2 + e^- \rightarrow 1s^2 2s + 2e^- \Rightarrow 1s^2 nl + 2e^- \Rightarrow 1s nl + 3e^-. \quad (18)$$

The IE-AI process is described by ionization of the $2s$ subshell with subsequent excitation of the $1s$ subshell and autoionization,

$$1s^2 2s^2 + e^- \rightarrow 1s^2 2s + 2e^- \Rightarrow \begin{cases} 1s 2s^2 \\ 1s 2s nl \end{cases} + 2e^- \Rightarrow 1s^2 + 3e^-. \quad (19)$$

The EI-AI process includes the excitation of B^+ with subsequent ionization and autoionization,

$$1s^2 2s^2 + e^- \rightarrow 1s 2s^2 nl + e^- \Rightarrow \begin{cases} 1s 2s^2 \\ 1s 2s nl \end{cases} + 2e^- \rightarrow 1s^2 + 3e^-, \quad (20)$$

$$1s^2 2s^2 + e^- \rightarrow 1s^2 2s nl + e^- \Rightarrow 1s 2s nl + 2e^- \rightarrow 1s^2 + 3e^-. \quad (21)$$

It is well known that the DW approximation often overestimates the electron-impact ionization and excitation cross sections for atoms and near neutral ions. The BED and binary-encounter-Bethe models for the CI and the scaled plane-wave Born approximation for the excitation were developed to study the cross sections for neutral atoms and near neutral ions [17,22,23]. Recently, the scaling factors were used to diminish the DW cross sections for the electron-impact ionization and excitation processes [24–26]. The following equation describes the scaled DW cross sections (σ^{CE^*}) for collisional excitation:

$$\sigma_{ik}^{\text{CE}^*}(\varepsilon) = \frac{\varepsilon}{\varepsilon + E_{ik} + \varepsilon_b} \sigma_{ik}^{\text{CE}}(\varepsilon), \quad (22)$$

where ε_b is the binding energy of the electron being excited, E_{ik} is a transition energy between level i and level k , and

$\sigma_{ik}^{\text{CE}}(\varepsilon)$ is the electron-impact excitation cross section. The scaled CI cross sections (σ^{CI^*}) are expressed by the following equation:

$$\sigma_{if}^{\text{CI}^*}(\varepsilon) = \frac{\varepsilon}{\varepsilon + I} \sigma_{if}^{\text{CI}}(\varepsilon), \quad (23)$$

where I is the ionization threshold of the ground state.

Energy levels, radiative and Auger transition probabilities, as well as electron-impact excitation and ionization cross sections are studied using the FLEXIBLE ATOMIC CODE [27], which implements the Dirac-Fock-Slater approach. Continuum orbitals of incident and scattered electrons are evaluated in the potential of ionizing and ionized ions for comparison with the experimental results. The electron-impact excitation and ionization processes are investigated using the distorted-wave approximation.

TABLE I. Theoretical ionization thresholds (in eV) for the B^+ ion. The NIST recommended values are presented for comparison. Single-configuration data (FAC1), results obtained using the configuration interaction method (FAC2). See the text for explanations.

Threshold	FAC1	FAC2	NIST [28]
SI	23.3	24.9	25.2
DI	61.1	62.5	63.1
TI	319.1	320.7	322.5

III. RESULTS

Single, double, and triple ionization thresholds for the B^+ ion are compared with the values provided by National Institute of Standards and Technology (NIST) [28] in Table I. It can be seen that the calculated ionization thresholds are slightly smaller than the NIST values. The difference between the calculated single-configuration and the NIST values varies from 1.9 eV for the SI threshold until 3.4 eV for the TI threshold. The difference for the DI threshold amounts to 2 eV.

According to NIST, the weight of the $B^+ 2s^2 \ ^1S_0$ configuration state function in the expansion of the intermediate wave function amounts to 93% [28]. The $B^+ 2p^2 \ ^1S_0$ configuration state function contributes 7%. Therefore, the correlation effects are included in the study of the single, double, and triple ionization using the configuration interaction method. The basis of interacting configurations for the ground state of the B^+ ion consists of the $2s^2$, $2p^2$, $3l^2$ ($l = 0-2$), $2p3p$, and $3s3d$ configurations. The correlation effects improve the theoretical ionization thresholds by adding ~ 1.6 eV to the single-configuration data (Table I).

Electron-impact SI cross sections obtained when continuum orbitals of incident and scattered electrons are evaluated in the potentials of ionizing and ionized ions are shown in Fig. 1. Data are presented for the ground $2s^2 \ ^1S_0$ and long-lived $2s^2 \ ^1S_0$ levels. The theoretical cross sections are

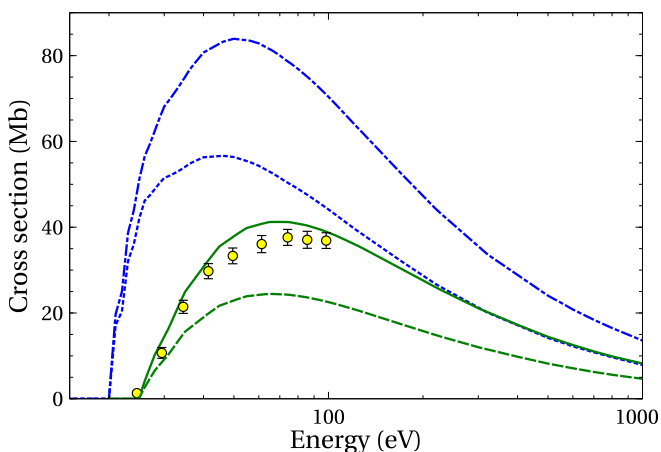


FIG. 1. Electron-impact SI cross sections for the ground $2s^2 \ ^1S_0$ (green) and long-lived $2s^2 \ ^1S_0$ (blue) levels of the B^+ ion. Solid and dot-dashed lines correspond to results obtained in the potential of the ionizing ion, dashed and dotted lines represent a study of the direct process in the potential of the ionized ion. Yellow circles with error bars: experiment for 9% of metastable fraction in the ion beam [8].

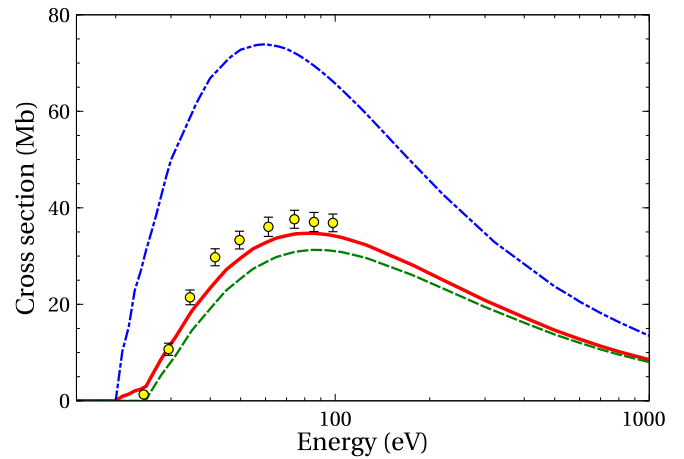


FIG. 2. The scaled electron-impact SI cross sections for the ground $2s^2 \ ^1S_0$ (green dashed) and long-lived $2s^2 \ ^1S_0$ (blue dot-dashed) levels of B^+ ion. Solid line (red) represents the scaled DW cross sections with a contribution of 91% from the ground level and 9% from the long-lived one. Yellow circles with error bars: experiment for 9% of the metastable fraction in the ion beam [8].

compared with measurements [8]. The contribution from the indirect process of SI is by two orders of magnitude lower as compared to the total SI cross sections. The electron-impact ionization cross sections for the long-lived $2s^2 \ ^3P_0$ level are in close agreement with data obtained for the $2s^2 \ ^3P_0$ level and, therefore, are not presented here. The experimental cross sections correspond to the 9% contribution from the long-lived levels of the $2s^2$ configuration. It should be noted that the correlation effects diminish the SI cross sections only by $\sim 2\%$. On the other hand, the correlation effects had a significant effect on the SI [29], DI [14], and TI [15] cross sections for other ions.

The SI cross sections for both ground and long-lived levels in case when continuum orbitals of incident and scattered electrons are evaluated in the potential of the ionizing ion are higher than those obtained in the potential of the ionized ion (Fig. 1). For the ground level, the theoretical cross sections evaluated in the potential of the ionizing ion give good agreement with experimental ones [8] at the energies near the SI threshold and a little beyond, but they are slightly higher at the peak value of the cross sections. However, as mentioned above, the experimental cross sections correspond to the 9% contribution from the long-lived levels [8]. The theoretical cross sections underestimate the experimental ones over the entire range of incident energies for the study in the potential of the ionized ion. The theoretical cross sections strongly overestimate experimental ones over the entire range of the energies for the levels of excited configuration in both studied potentials (Fig. 1).

The scaled SI cross sections for the ground and long-lived levels of the B^+ ion are compared with experimental ones [8] in Fig. 2. It can be seen that the scaled DW cross sections calculated for the ground $2s^2 \ ^1S_0$ level in the potential of the ionizing ion are lower than measurements over the entire range of the energies. It should be noted that the cross sections calculated in the potential of the ionized ion strongly underestimate the experimental ones and are not presented here.

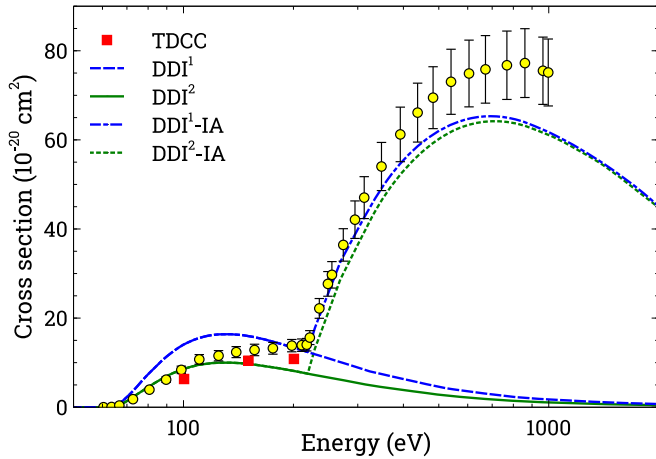


FIG. 3. Electron-impact DI cross sections for the ground level of the B^+ ion. Configurations with vacancy in the $1s$ subshell are not included in the study of the DDI process. DDI^1 : CI cross sections obtained in the potentials of the ionizing ions; DDI^2 : $B^+ \rightarrow B^{2+}$ CI cross sections obtained in the potential of the ionizing ion but $B^{2+} \rightarrow B^{3+}$ CI cross sections obtained in the potential of the ionized ion; DDI^1 -IA: sum of DDI^1 and IA cross sections; DDI^2 -IA: sum of DDI^2 and IA cross sections. TDCC: previous calculations [11]. Yellow circles with error bars: experiment for 9% of the metastable fraction in the ion beam [30].

For the long-lived $2s2p^3P_0$ level, the theoretical scaled cross sections evaluated in the potential of the ionizing ion strongly overestimate the experimental ones over the entire range of energies. The theoretical cross sections corresponding to the 9% fraction of the long-lived levels in the ion beam show a reasonable agreement with measurements (Fig. 2).

Electron-impact DI cross sections for the B^+ ion are compared with measurements [30] in Fig. 3. Calculations are performed for the ground level of the B^+ ion using the scaled DW cross sections. The total DI cross sections are studied as a sum of the DDI and IA processes. Configurations with vacancy in the $1s$ subshell are not included in the study of the DDI process. Previous calculations using the TDCC approach for the DDI process also did not include the $1s$ subshell [11]. An extrapolation of the DDI cross sections was adopted starting from the $1s$ subshell ionization threshold [11]. In this paper, the CI cross sections for the ionization from the levels of the B^+ ion are investigated in the potential of the ionizing ion. The potentials of the ionized and ionizing ions are used to analyze the CI process from the levels of the B^{2+} ion produced by the ionization from the B^+ ion. The DDI cross sections obtained in the potentials of the ionizing ions are by $\sim 6 \times 10^{-20} \text{ cm}^2$ higher compared to the theoretical values calculated in the potentials of the ionizing and ionized ions (Fig. 3). The TDCC result is slightly lower than the measurements. The theoretical DDI cross sections obtained in the potentials of the ionizing and ionized ions are in good agreement with experiment at the lower energies of the incident electron. The DDI cross sections studied in the potentials of the ionizing ions at energies close to the ionization threshold of the $1s$ subshell show a good agreement with measurements.

Quite good agreement with measurements is provided in both cases of theoretical calculations for total DI at the en-

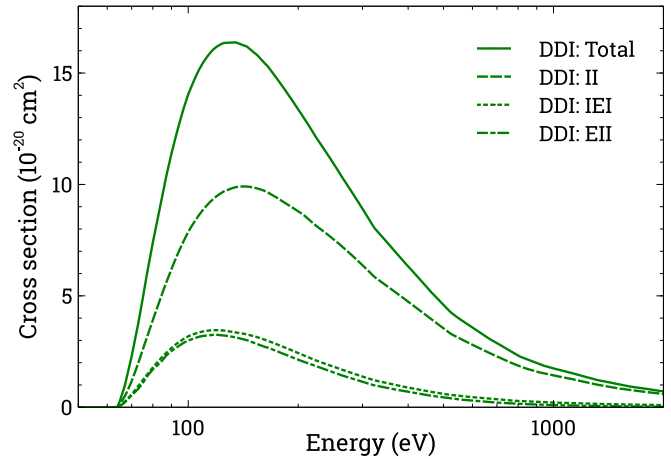


FIG. 4. Contribution of various multistep paths to the total DDI process of the B^+ ion. See explanations in the text for the listed processes.

ergies beyond the inner-shell ionization threshold (Fig. 3). However, the theoretical cross sections start to decrease faster than experimental ones resulting in a significant disagreement at the peak and beyond where the theoretical DI cross sections strongly underestimate the experimental ones. It shows that some additional ionization processes, which are missing in the above presented study, should be taken into account.

Contribution of various pathways to the electron-impact DDI process for the B^+ ion is shown in Fig. 4. It can be seen that the II path dominates over IEI and EII. The II contributes $\sim 70\%$ to the total DDI cross sections. The contribution of IEI is a little higher but comparable to that of EII.

The DDI study is extended by including ionization from the $1s$ subshell of configurations of the B^{2+} ion. The produced configurations of the B^{3+} ion with a single vacancy in the $1s$ subshell are below the TI threshold. The results of this extension are presented in Fig. 5. It can be seen that an increase in the DDI cross sections at larger energies due to the contribution of the ionization from the $1s$ subshell of the

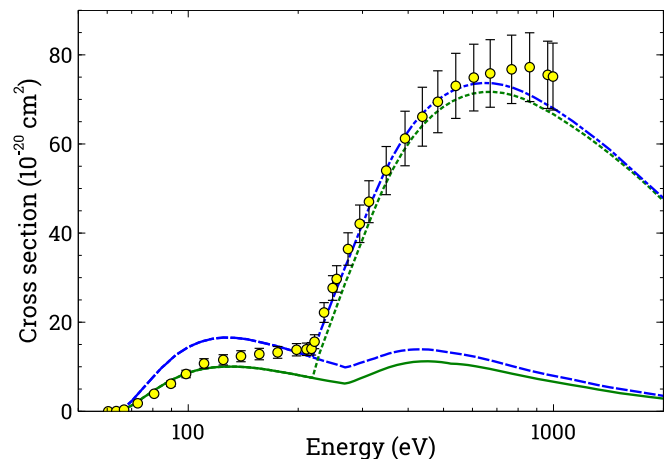


FIG. 5. Same as Fig. 3 but includes ionization from the $1s$ subshell of the B^{2+} ion for the DDI process. See explanations in the text.

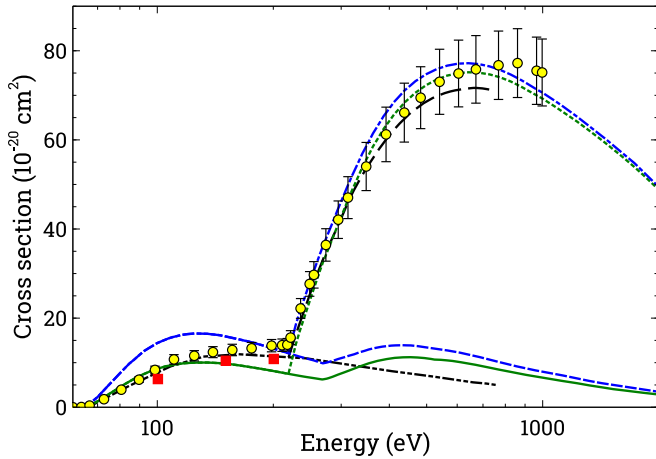


FIG. 6. Same as Fig. 5 but with the EI-AI and IE-AI processes included. Solid squares (red): TDCC calculations [11]; dashed-fine line (black): configuration average distorted-wave (CADW) calculations for the single ionization of the $1s$ subshell of the ground configuration added to a background of TDCC fit (black dashed-dot-dot line). See explanations in the text.

B^{2+} ion leads to a better agreement for the total theoretical DI cross sections with experimental results.

The contribution of the additional EI-AI and IE-AI processes [Eqs. (7) and (8)] leads to even better agreement with experimental cross sections at higher energies of the incident electron (Fig. 6). Comparison with the previous calculations [11] which used the TDCC method for DDI and CADW for the indirect DI process is also presented. The current values are slightly above the previous calculations. It can be explained by the fact that extrapolation of the DDI cross sections was employed beyond the $1s$ subshell ionization threshold. That could lead to some inaccuracies in their DDI values. Furthermore, their DDI calculations missed the $1s$ subshell. This shows that role of the EI-AI and IE-AI processes is important in the DI of B^+ . The IE-AI and EI-AI processes involve excitations from the $1s$ subshell. For EI-AI, this corresponds to the excitations to the $B^+ 1s2s^2nl$ ($n \leq 4$, $l \leq n$) configurations with subsequent ionization from the $2s$ or nl subshells [e.g., (21)]. The produced configurations are subject to autoionization. It should be noted that convergence of the cross sections has to be studied for the electron-impact excitation in order to obtain the reliable data. The previous investigations for tungsten ions with the open $4f$ subshell in the ground configurations demonstrated the importance of the high- nl excitations for the indirect SI process [31–36]. Channels corresponding to the excitations to the shells with the principal quantum number $n > 4$ contribute $\sim 3\%$ to the total excitation cross sections for the B^+ ion. For IE-AI, the ionization from the $2s$ subshell of the B^+ ion leads to the $1s^22s$ configuration. The excitations from the $1s$ subshell of B^{2+} produce the autoionizing configurations which decay to the states of the B^{3+} ion [e.g., (19)]. The cross sections for the IE-AI process reach $\sim 4 \times 10^{-20} \text{ cm}^2$ at peak ($\sim 400 \text{ eV}$) whereas EI-AI leads to values by an order of magnitude lower.

It should be noted that the IE-AI and EI-AI processes end by autoionization instead of CI. The CI from autoionizing

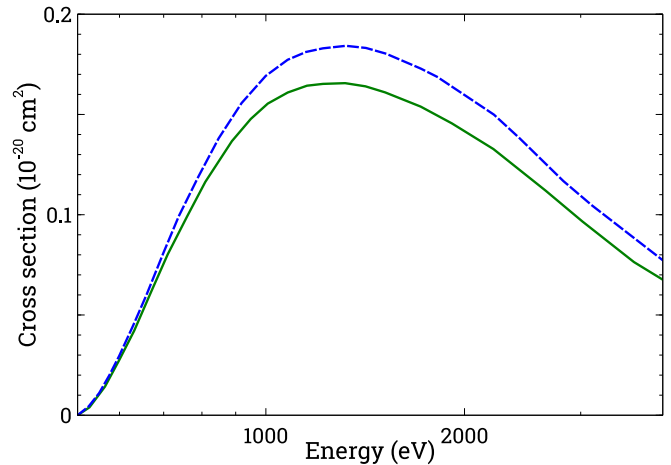


FIG. 7. Electron-impact TI (DDI-AI) cross sections for the B^+ ion. See explanations in the text.

configurations produced by the initial IE and EI processes corresponds to the IEI and EII paths of the DDI process. However, not all autoionizing states of the B^{2+} ion reach the B^{3+} ion in the final steps of IEI and EII since the final CI is determined by the probability that is lower than one [see Eqs. (5) and (6)]. On the other hand, all autoionizing states of the B^{2+} ion lead to the B^{3+} ion through Auger transitions. This explains why the $1s$ subshell of B^{2+} is not included in the initial study of the DDI process presented in Fig. 3. Excitations and ionizations from the $1s$ subshell are studied separately since this leads to the autoionizing states, populations of which are thoroughly wiped out by the Auger transitions. Furthermore, the ionization from the $1s$ subshell of the B^+ ion produces the autoionizing states that decay through the Auger transitions to B^{3+} . However, part of these states leads to B^{3+} through CI by the scattered or ejected electrons in the II or IEI paths of the DDI process. These processes, i.e., DDI(II) and DDI(IEI) that include the initial ionization from the $1s$ subshell of B^+ , compete with IA to reach the states of B^{3+} first. The final CI in the DDI process from the autoionizing states should occur quicker compared to the Auger transition if it is assumed that interaction with the bound electrons takes place instantly. However, as mentioned above, not all populations of the autoionizing states of the B^{2+} ion are destroyed by the final CI in the DDI process and decay further through Auger transitions. In both cases the states of the B^{3+} ion are reached. Therefore, the produced autoionizing states are only analyzed by considering the Auger transitions from them since it leads to a transfer of all population to the B^{3+} ion. The study of only the DDI process that involves the autoionizing states would lead to lower cross sections compared to IE-AI, EI-AI, and IA.

Previously, it has been demonstrated for the Se^{2+} and Se^{3+} ions that the AI process following DDI leads to the TI [14,15]. Therefore, the TI process is studied for the B^+ ion by considering DDI with subsequent autoionization. The sequential ionization from the $1s$ subshell of the B^+ ion leads to the $B^{3+} 2s^2$ configuration that decays to B^{4+} . Only the theoretical TI cross sections are presented in Fig. 7. The two

cases of potentials are studied for the TI cross sections. The TI cross sections are by two orders of magnitude lower as compared to the DI cross sections. It can be seen that peak of the cross sections is reached at ~ 1300 -eV energy with the maximum value of $0.18 \times 10^{-20} \text{ cm}^2$ for the study in the potentials of the ionizing ions. The calculations in the ionizing and ionized potentials are $\sim 0.6\%$ lower compared to the study in the ionizing potentials. Experimental results are needed in order to determine which case describes the TI process more accurately.

Finally, the largest difference among experimental values and theoretical ones is obtained for the DDI cross sections below the $1s$ subshell ionization threshold. The uncertainty amounts to $\sim 50\%$ in this energy region. A similar value is obtained for the difference between theoretical results studied in different potentials (Fig. 6). A much better agreement with measurements is obtained for energies beyond the $1s$ subshell ionization threshold. The calculated DI and TI cross sections for the different potentials agree within $\sim 10\%$ for peak values.

IV. CONCLUSIONS

Electron-impact single, double, and triple ionization cross sections are studied for the ground level of the B^+ ion. The study includes correlation effects for the ground configuration of the B^+ ion and scaled DW cross sections for the

electron-impact excitation and ionization processes. A good agreement with experimental SI results is achieved for the study in the potential of the ionizing ion using the scaled DW cross sections.

The DI study combines direct and indirect processes. Ionization from the $1s$ subshell with subsequent autoionization determines the DI cross sections for the indirect process. The II, IEI, and EII paths of the DDI process are considered. What is more, the EI-AI and IE-AI processes that involve excitations from the $1s$ subshell are included in the study. The added contribution from these processes provides better agreement with measurements at the high-energy side. Only DDI is responsible for the formation of states of the B^{3+} ion for the energies from the DI threshold up to SI threshold of the $1s$ subshell. The II path of the DDI process dominates over the IEI and EII paths.

The DDI process that involves sequential ionization from the $1s$ subshell produces autoionizing $2s^2$ configuration of the B^{3+} ion that decays to B^{4+} . The TI cross sections are by two orders of magnitude lower as compared to the DI cross sections for the B^+ ion.

ACKNOWLEDGMENT

Part of the computations was performed on resources at the High Performance Computing Center “ŽHPC Saulėtekis” in Vilnius University Faculty of Physics.

-
- [1] A. Müller, *Phys. Lett. A* **113**, 415 (1986).
 [2] M. Hahn and D. W. Savin, *Astrophys. J.* **800**, 68 (2015).
 [3] E. Vangioni-Flam, M. Casse, and J. Audouze, *Phys. Rep.* **333**, 365 (2000).
 [4] R. Lunsford, V. Rohde, A. Bortolon, R. Dux, A. Herrmann, A. Kallenbach, R. M. McDermott, P. David, A. Drenik, F. Laggner, R. Maingi, D. K. Mansfield, A. Nagy, R. Neu, E. Wolfrum, and the ASDEX Upgrade team, *Nucl. Fusion* **59**, 126034 (2019).
 [5] J. Li, Y. Zhao, X. Gu, C. Li, B. Wan, X. Zhang, J. Luo, X. Gong, J. Xie, Y. Wan, P. Qin, X. Wang, Y. Meng, S. Li, X. Gao, Y. Yang, D. Xue, Y. Mao, X. Den, and W. Shen, *Nucl. Fusion* **39**, 973 (2002).
 [6] J. C. Berengut, S. D. Loch, M. S. Pindzola, C. P. Ballance, and D. C. Griffin, *Phys. Rev. A* **76**, 042704 (2007).
 [7] K. Wang, O. Zatsarinny, and K. Bartschat, *Phys. Rev. A* **93**, 052715 (2016).
 [8] J. C. Berengut, S. D. Loch, M. S. Pindzola, C. P. Ballance, D. C. Griffin, M. Fogle, and M. E. Bannister, *Phys. Rev. A* **78**, 012704 (2008).
 [9] O. Voitke, N. Djurić, G. H. Dunn, M. E. Bannister, A. C. H. Smith, B. Wallbank, N. R. Badnell, and M. S. Pindzola, *Phys. Rev. A* **58**, 4512 (1998).
 [10] R. A. Falk, G. Stefani, R. Camilloni, G. H. Dunn, R. A. Phaneuf, D. C. Gregory, and D. H. Crandall, *Phys. Rev. A* **28**, 91 (1983).
 [11] M. S. Pindzola, J. A. Ludlow, C. P. Ballance, F. Robichea, and J. Colgan, *J. Phys. B: At., Mol. Opt. Phys.* **44**, 105202 (2011).
 [12] V. Jonauskas, A. Pranciševičius, Š. Masys, and A. Kynienė, *Phys. Rev. A* **89**, 052714 (2014).
 [13] J. Koncevičiūtė and V. Jonauskas, *Phys. Rev. A* **93**, 022711 (2016).
 [14] J. Koncevičiūtė, S. Kučas, Š. Masys, A. Kynienė, and V. Jonauskas, *Phys. Rev. A* **97**, 012705 (2018).
 [15] J. Koncevičiūtė, S. Kučas, A. Kynienė, Š. Masys, and V. Jonauskas, *J. Phys. B: At., Mol. Opt. Phys.* **52**, 025203 (2019).
 [16] V. Jonauskas and Š. Masys, *J. Quant. Spectrosc. Radiat. Transfer* **229**, 11 (2019).
 [17] Y.-K. Kim and M. E. Rudd, *Phys. Rev. A* **50**, 3954 (1994).
 [18] F. Zhou, Y. Ma, and Y. Qu, *Phys. Rev. A* **93**, 060501(R) (2016).
 [19] Y. Ma, F. Zhou, L. Liu, and Y. Qu, *Phys. Rev. A* **96**, 042504 (2017).
 [20] Y. Ma, Z. Liu, F. Zhou, and Y. Qu, *Phys. Rev. A* **98**, 043417 (2018).
 [21] Y. Ma, L. Liu, Y. Wu, Y. Qu, and J. Wang, *Phys. Rev. A* **101**, 052703 (2020).
 [22] Y.-K. Kim, *Phys. Rev. A* **64**, 032713 (2001).
 [23] Y.-K. Kim and P. M. Stone, *Phys. Rev. A* **64**, 052707 (2001).
 [24] V. Jonauskas, *Astron. Astrophys.* **620**, A188 (2018).
 [25] A. Kynienė, S. Kučas, S. Pakalka, Š. Masys, and V. Jonauskas, *Phys. Rev. A* **100**, 052705 (2019).
 [26] V. Jonauskas, *At. Data Nucl. Data Tables* **135**, 101363 (2020).
 [27] M. F. Gu, *Can. J. Phys.* **86**, 675 (2008).
 [28] A. Kramida, Y. Ralchenko, J. Reader, and NIST ASD Team, NIST Atomic Spectra Database (ver. 5.8), 2020.
 [29] V. Jonauskas, A. Kynienė, S. Kučas *et al.*, *Phys. Rev. A* **100**, 062701 (2019).
 [30] V. P. Shevelko, H. Tawara, F. Scheuermann, B. Fabian, A. Müller, and E. Salzborn, *J. Phys. B: At., Mol. Opt. Phys.* **38**, 525 (2005).

- [31] D.-H. Zhang and D.-H. Kwon, *J. Phys. B: At., Mol. Opt. Phys.* **47**, 075202 (2014).
- [32] V. Jonauskas, A. Kynienė, G. Merkelis, G. Gaigalas, R. Kisielius, S. Kučas, Š. Masys, L. Radžiūtė, and P. Rynkun, *Phys. Rev. A* **91**, 012715 (2015).
- [33] A. Kynienė, Š. Masys, and V. Jonauskas, *Phys. Rev. A* **91**, 062707 (2015).
- [34] A. Kynienė, S. Pakalka, Š. Masys, and V. Jonauskas, *J. Phys. B: At., Mol. Opt. Phys.* **49**, 185001 (2016).
- [35] A. Kynienė, G. Merkelis, A. Šukys, Š. Masys, S. Pakalka, R. Kisielius, and V. Jonauskas, *J. Phys. B: At., Mol. Opt. Phys.* **51**, 155202 (2018).
- [36] F. Jin, A. Borovik, B. Ebinger, and S. Schippers, *J. Phys. B: At., Mol. Opt. Phys.* **53**, 075201 (2020).